The stiffness of a roller between two flat surfaces

An experimental study using modal analysis

Wijnberg, David Onno; Eling, Rob; van Ostayen, Ron A.J.

DOI
10.1016/j.triboint.2025.111234

Publication date
2026

Document Version
Final published version

Published in
Tribology International

Tribology International 214 (2026) 111234

Contents lists available at ScienceDirect

Tribology International

journal homepage: www.elsevier.com/locate/triboint

Full Length Article

The stiffness of a roller between two flat surfaces: An experimental study using modal analysis

David Onno Wijnberg [a], Rob Eling [b], Ron A.J. van Ostayen [a,*]

[a] Department of Precision and Microsystems Engineering, Delft University of Technology, Mekelweg 2, Delft, 2628 CD, The Netherlands
[b] PM B.V., Galileistraat 2, Dedemsvaart, 7701 SK, The Netherlands

ARTICLE INFO

Keywords:
Roller stiffness
Contact stiffness
Roller bearing
Surface roughness
Line contact
Hertz contact
Tripp

ABSTRACT

The load-stiffness relationship of a roller sandwiched between two flat surfaces is experimentally investigated. This study provides a comprehensive and well-documented dataset on roller stiffness in bearing applications. The measurements, obtained using hammer impact tests on a variety of rollers are both accurate and precise. Comparing the experimental results with the predictions from the commonly used Tripp model, we observe that the stiffness of the roller under relatively light load conditions is significantly lower than what is predicted by the Tripp model. This discrepancy is primarily attributed to surface roughness, a factor not accounted for in the Tripp model. For practical engineering applications, we propose simple formulas that predict the stiffness of real-world roller-rail contacts with an accuracy of ±10%.

1. Introduction

In many cases, it is important to be able to quantify the stiffness of bearings. For example, because it can influence the positioning error or the eigenfrequencies of a machine or mechanism. A single rolling element compressed between two flat rails is the fundamental building block for modeling rolling bearing assemblies. For spherical rolling elements, Hertz' theory is an accurate analytic approach to model the stiffness of most real contacts. However, for a cylindrical roller-rail contact, many factors come into play. In particular: roller profiling, misalignment, traction, surface roughness and the arbitrary choice of an evaluation depth. This makes modeling difficult and ambiguous.

Previous research resulted in many analytic load–deflection relations for cylindrical roller-rail contacts. Teutsch and Sauer [1] give an overview of the most common relations and compares these. In their case study, most of these relations yield similar results. The analytical model as presented by Tripp is the most commonly applied model. This model considers a 2D cylinder compressed between two half-spaces, and is thus based on the assumption of plane-strain and a half-space.

Another model presented by Palmgren [2] is used by many authors [1,3–6]. They all assume this relation to be based on laboratory testing of rollers loaded against raceways. However, as Nikpur and Gohar [7] points out, this load–deflection relation is merely a simplification of the analytical solution presented by Lundberg [8].

Although many theoretical models are presented in the literature, only very few experimental validations are performed. Traditionally, load–deflection relations are obtained by statically loading a roller between two flat bodies and measuring the displacement. This method is used by various authors, often with discrepancies between measurement and theory of more than 40.000% [9]. Or, the rollers used are profiled [7,10] and the quality of the rollers and rail is not specified.

Sherif [3] proposed and demonstrated a promising experimental method to measure the stiffness of a roller between two flat surfaces using modal analysis. However, the asymmetric test setup inherently leads to misalignment, resulting in measurement errors. In addition, the limited inertia of the setup results in a relatively large contribution of the inertia of the roller itself in the overall dynamics, which is not taken into account. Moreover, the setup requires an assumption of zero deformation of the setup base.

In the current state of research, many researchers claim to have a good model to predict the stiffness of line contacts. However, the experimental validation of these models is very limited. It lacks a well-documented empiric load-stiffness relation for cylindrical roller-rail contacts. Recent work by Hu et al. [11] addresses several of these limitations by introducing a refined line-contact model based on a slice-by-slice half-space formulation. Their model accounts for non-uniform deformation, edge effects, and surface roughness—factors often neglected in classical formulations like Tripp or Palmgren. Although they report good agreement with finite element results for tapered roller bearings, their approach is not directly applicable to cylindrical

* Corresponding author.
E-mail address: R.A.J.vanOstayen@tudelft.nl (R.A.J. van Ostayen).
URL: https://www.tudelft.nl/staff/r.a.j.vanostayen (R.A.J. van Ostayen).

https://doi.org/10.1016/j.triboint.2025.111234
Received 17 May 2025; Received in revised form 15 September 2025; Accepted 23 September 2025
Available online 26 September 2025

(a) CAD model (b) Picture (c) CAD model top view

Fig. 1. The test setup used for the experiments. Three rail pairs are bolted to the two masses. The rollers are placed between the rails. Compression springs apply a controllable load on the rollers-rails contacts. An impact hammer delivers impulse to the upper disc and the resulting frequency response is measured by accelerometers. The setup is isolated from external influences by an inflatable rubber tube.

rollers in flat rail contact, where the geometry, boundary conditions, and contact behavior differ significantly. This paper presents such an empiric relation based on hammer impact measurements.

Experiments are performed on steel cylindrical bearing rollers in the range of 1.5–9.0 mm in diameter and 1.4–8.8 mm in length, in contact with flat steel rails. Variations of load, material, surface roughness, and roller geometry are investigated. A setup is presented in which rollers are compressed between flat rails. Hammer impact measurements are performed to measure the effective roller-rail stiffness under a compressive load that can be varied in a controlled manner.

2. Material and methods

This section describes the experimental setup, the procedure used for hammer impact measurements, and the approach to isolating the roller-rail contact dynamics from the rest of the setup. In addition, the rationale for choosing hammer impact over static displacement measurements is discussed, and validation steps taken to ensure the accuracy of the results are outlined.

2.1. Experimental setup

The test setup (Fig. 1) consists of six flat steel rails ②, bolted ⑨ to two heavy steel discs ①. Each pair of rails compresses one roller ③ under a controlled load. The dimensions of the rails are provided in Fig. 14, while the specifications of the rollers used are listed in Table 1. The load is applied using four pairs of compression springs ⑧, which are compressed by threaded rods ④ with star knob nuts ⑦.

A rectangular cage mounted on the rails ensures roller alignment parallel to their length. An inflatable rubber tube isolates the setup from external influences (Fig. 1(b)). The steel discs are chosen as they are both stiff and heavy, ensuring that the frequencies of their rigid body modes are well-separated from the flexible body modes, which occur above 2000.000 Hz. This minimizes interference in the measured dynamics. To ensure proper alignment of the rails and rollers, the steel discs are ground flat. Furthermore, the point symmetric and well-constrained design of the rail placement ensures uniform load distribution and symmetry of eigenmodes, which contributes to the overall stability and repeatability of the measurements. Table 2 lists all components used.

2.2. Equipment

The frequency response function (FRF) was measured using four tri-axial accelerometers (PCB Piezotronics model 356A16). Their positions were determined based on a pre-study with a simplified FEM model, ensuring that the dominant eigenmodes would be observable at these locations. Measurements confirmed that the expected mode shapes could indeed be distinguished. To verify robustness, the accelerometers were also displaced radially by ±50%, which showed that all relevant modes within the frequency range of interest (0.000 Hz–2000.000 Hz) remained detectable. In addition, the hammer impact location was varied to guarantee sufficient excitation of all modes. On the top disk, three accelerometers (labeled as ⑤ in Fig. 1(c)) are mounted directly above the rollers; specifically, each one is placed between a pair of bolts, at a distance of 80.000 mm from the center of the disks. On the bottom disk, a single accelerometer is placed at the center of the underside of the disk. The impulse is applied using a PCB Piezotronics 086D05 impact hammer with an 084B04 tip (at location ⑥ in Fig. 1(a)). All data is recorded using a PAK MKII measurement system, configured with a sampling rate of 20 480.000 Hz and a window length of 3.2 s. Surface roughness of the rollers and rails is measured using a Mitutoyo SJ-210 portable surface roughness tester, configured to evaluate parameters according to ISO 4287:1997. The roundness and cylindricity are measured with a Mahr MarForm MMQ. The recorded data is analyzed using MATLAB [12].

2.3. Procedure

The measurements were carried out on various roller types under a range of load conditions. The initial load consisted of the weight of the upper disc and rails. This load was incrementally increased by tightening the star knobs ⑥ in steps of 180.000°, up to 30.000% of the static load rating of the roller as specified in ISO 14728-2:2017. At each load step, three hammer impacts were applied, and the resulting frequency responses were measured and averaged. The test procedure was repeated three times for each roller type. Between repetitions, the upper disk was removed, and the rollers were slightly rotated by approximately ±5.000° to renew the contact area, ensuring consistent surface conditions.

2.4. Isolating the roller-rail contact from the rest of the setup

The deformation of a half-space can only be specified relative to a selected point of reference in that half-space [13].

To analytically estimate the deformation at the contact, Tripp's closed-form expressions are used for both the roller and the rail, treating each as a semi-infinite elastic body.

For the roller, the vertical displacement under load P per contact length is given by Johnson [13]:

$$\delta_{roller} = 4P\frac{1-\nu_{roller}^2}{\pi E_{roller}}\left\{\ln\left(\frac{4R}{a}\right)-\frac{1}{2}\right\} \tag{1}$$

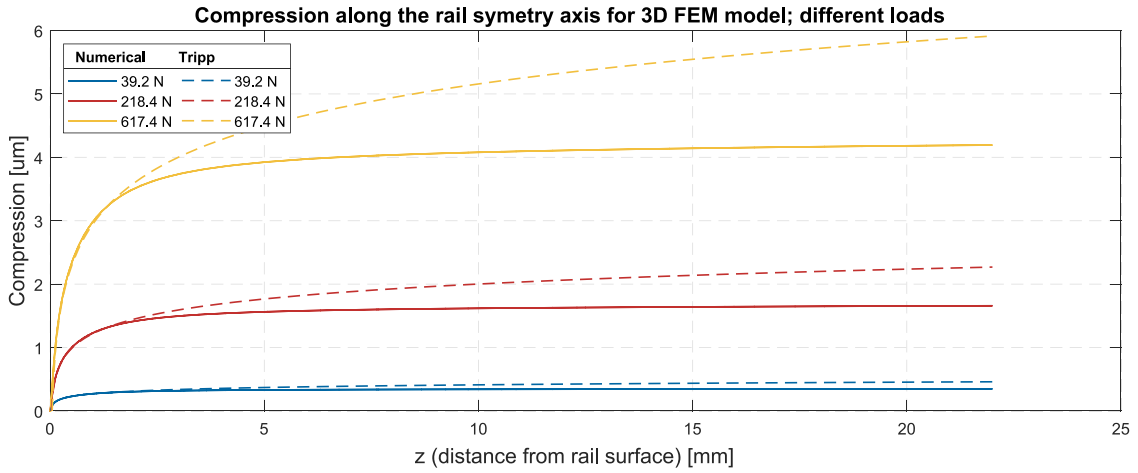

Fig. 2. Graph of compression of the rail along the symmetry axis: 3D Numerical and analytic results for roller type 1 variation of load.

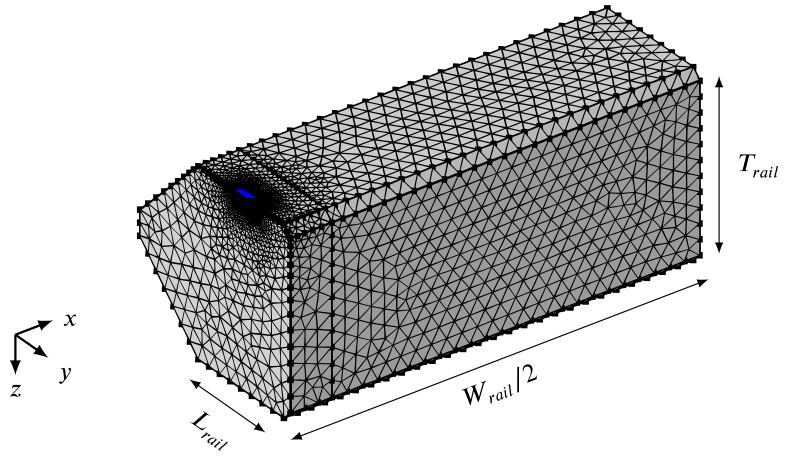

Fig. 3. Rail Geometry of 3D finite element model; compression of a rail of thickness T_{rail}, length L_{rail} and width W_{rail}. The rail is loaded over a length of L_{we} by an applied pressure.

For the rail, the simplification is made that it behaves as a half-space evaluated at a finite depth $d = t$, where t is the thickness of the rail segment involved in the contact. This leads to the following approximation:

$$\delta_{rail} = P\frac{1-\nu_{rail}^2}{\pi E_{rail}}\left\{2\ln\left(\frac{2t}{a}\right) - \frac{\nu_{rail}}{1-\nu_{rail}}\right\} \tag{2}$$

Here, R is the roller radius, a is the contact radius, and E and ν are the Young's modulus and Poisson's ratio of the respective material. The contact radius a and the effective modulus E^* are defined by:

$$a = \sqrt{\frac{4PR}{\pi E^*}} \quad \text{and} \quad E^* = \frac{1-\nu_{roller}^2}{E_{roller}} + \frac{1-\nu_{rail}^2}{E_{rail}} \tag{3}$$

As $a \ll t$, this assumption is an appropriate estimate, though arbitrary when the objective is to exactly solve the problem. The majority of the strain will take place in the vicinity of the contact; the impression scales with $\ln t$. In practical assemblies a datum of zero impression does not exist as the whole system has some compliance.

Furthermore, the remainder of the setup has a finite stiffness. In order to identify the stiffness of the roller-rail contacts, the stiffness of the rest of the setup has to be deducted.

Fig. 2 shows how in the rail, in region near the contact, the numerical and Tripps model greatly agree. In this region, stresses are dominantly prescribed by the concentrated contact. Further from the contact, stress diminishes significantly. In this region, the system's geometry becomes a dominant factor influencing the deformations. This is also corroborated by Fig. 4, showing displacements in a rail with a fixed bottom under a load applied by a type-1 roller. An isoline is plotted at 10% of the contact displacement. 90% of the displacement in the z-direction occurs within the region enclosed by the isoline. Outside this region, the Von Mises stress drops to less than 1% of its peak value. Similarly, the elastic strain energy density decreases to less than 0.01% of its peak value.

Modeling entire assemblies in full detail using FEM, including contact conditions, is computationally expensive and thus impractical.

To efficiently and accurately model an assembly containing roller-rail contacts, this study proposes to place simple bodies in the two contact regions where each roller contacts the rest of the assembly. These two bodies are modeled as rigid and connected by a spring element. The stiffness of these springs (k) is derived from Tripp, calculating the stiffness for a roller and two half spaces with an evaluation depth equal to the thickness of the rigid bodies. The rest of the rail geometry is modeled with a 3D FEA. The choice of the geometry of the simple rigid body can be user-defined. For this specific model a disc with a thickness of 3.000 mm and a radius of 4.000 mm is selected, encompassing approximately 90% of the displacement.

For the tested geometries, this hybrid approach — combining partial numerical and analytical modeling — was compared to a fully meshed FEM model that includes contact conditions, and it produced closely matching results.

In the 3D FEM analysis using COMSOL, symmetry was applied to model only half of the rail geometry, with the symmetry plane indicated

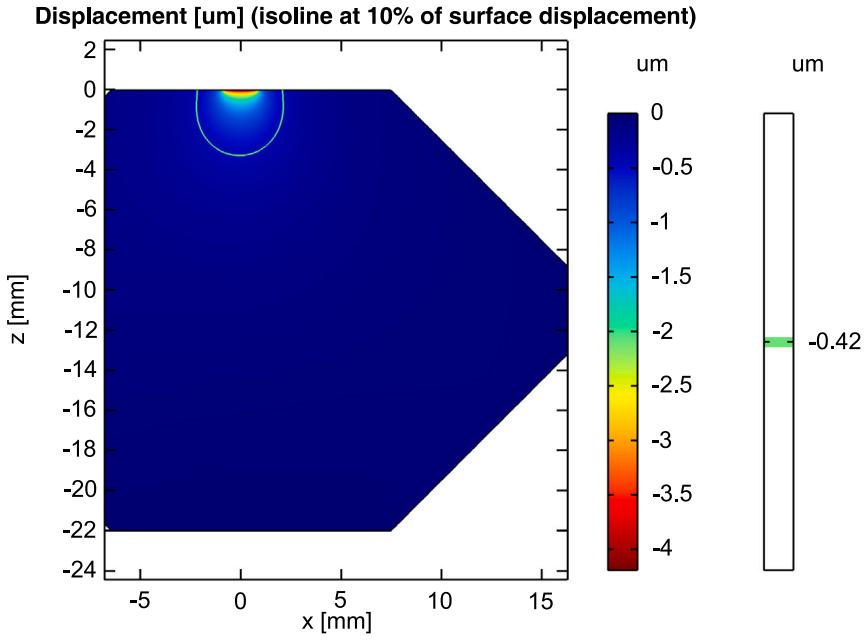

Fig. 4. Displacement in the plane of symmetry of the 3D rail geometry under a 617.4 N load applied by roller type 1.

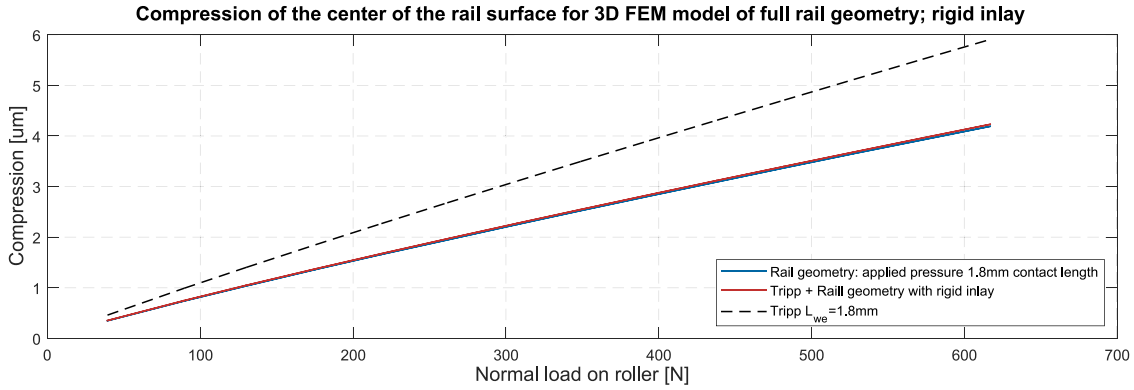

Fig. 5. Graph of compression of the rail along the symmetry axis: 3D Numerical of full rail geometry vs. combination of a rigid inlay and analytical compression.

in Fig. 4. The bottom of the rail was fixed to simulate a rigid support. The meshed geometry is shown in Fig. 3, where the contact region — highlighted in blue — indicates the area where pressure was applied. A mapped mesh with quadrilateral elements was used in this region, while the rest of the rail volume was meshed with tetrahedral elements.

Fig. 5 illustrates the compression behavior of both the full numerical model and the hybrid model (rigid inlay with analytical compression), highlighting the strong agreement between the two.

The bolt connections between the rails and discs are assumed to have negligible deformation, with drilled and threaded holes modeled as rigid. Contact between the rail and disc is simulated with and without friction, showing no difference. Stress stiffening within the setup increases its stiffness by approximately 25.000%.

If the setup components are considered to be rigid, the natural frequency of this system is that of an idealized two mass spring system with the natural frequency $\omega_0 = \sqrt{\frac{6k}{m}}$. Here, m is the combined mass of a single disc, attached rails, and bolts, while k represents the stiffness of a single roller in series with two rail components. In this FEM model k is swept over a large range. When the eigenfrequencies of the 3D FEA are calculated, the deviation from a perfect two mass spring system can be quantified.

The FEA found the compliance of the setup accurately modeled as a constant stiffness in series with k, as described in Eq. (4). With ω_0 found in the analysis and $3k$ predefined, K_{setup} can be calculated. The stiffness of the setup (K_{setup}) is found to be $1.45 \cdot 10^9$ N/m.

$$\omega_0 = \sqrt{\frac{2k_{total}}{m}}, \qquad \text{with} \quad \frac{1}{K_{total}} = \frac{1}{3k} + \frac{1}{K_{setup}} \tag{4}$$

Fig. 6 shows the relevant mode shapes for a stiffness corresponding to a 440.000 N load on a roller type 1. The measured stiffness values are shown in Fig. 8, and the corresponding transfer function is presented in Fig. 7. The eigenfrequencies from the model closely match the measured values. The dynamic mode that is dominated by the normal translation in the z-direction, shown in Fig. 6(b), has a frequency of 745.000 Hz, and in the shown transfer function the corresponding mode is measured at 748.000 Hz. The tilt modes have a frequency of 581.000 Hz in the FEM analysis, and in the measured response, these modes are centered around 584.000 Hz. The first flexible body modes appear above 2250.000 Hz, well separated from the rigid body dynamics.

2.5. Hammer impact versus static displacement measurements

The stiffness of a roller can also be measured using static displacement, where a known force is applied, and displacement is directly measured. As shown in Fig. 8, both methods yield consistent stiffness values, but static displacement measurements exhibit significantly

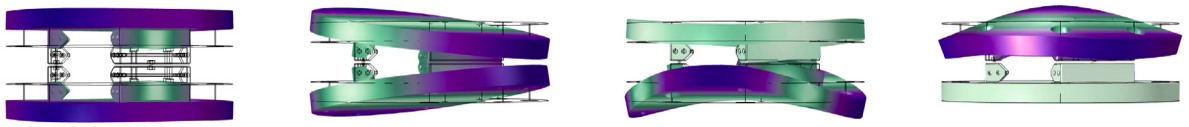

(a) First eigenmode, normal translation: 745.000 Hz (b) Second eigenmode type, tilt: 581.000 Hz (c) Third eigenmode type, flex mode: 1873.000 Hz (d) Fourth eigenmode type, flex mode: 2728.000 Hz

Fig. 6. Plots for the various mode shapes. The stiffness per spring element is $4.65 \cdot 10^7$ N/m.

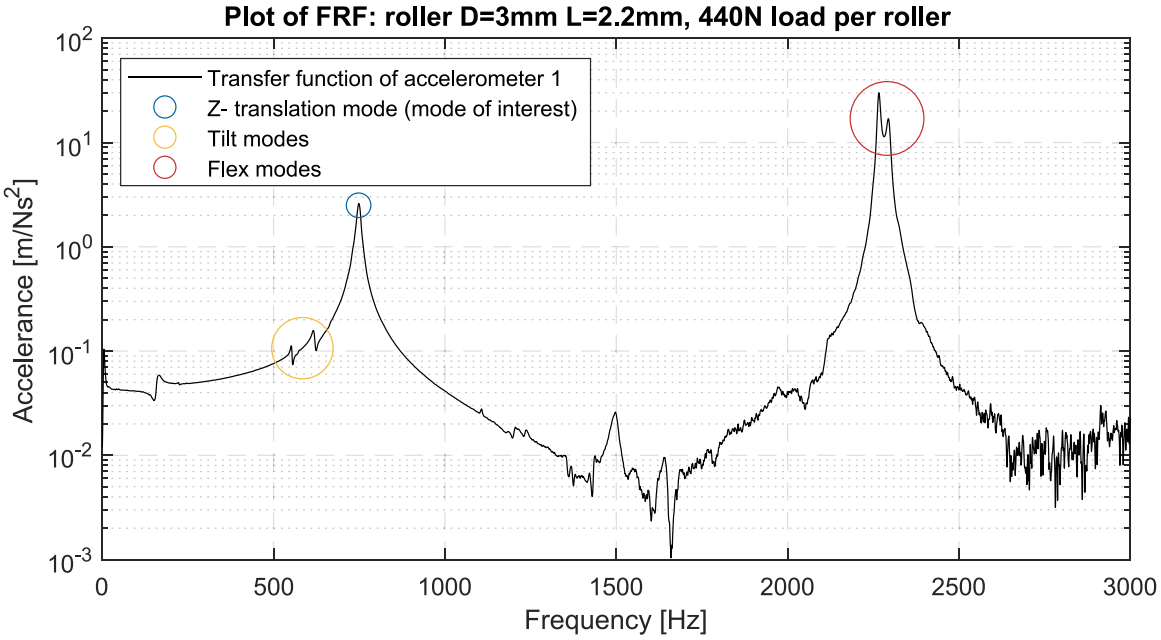

Fig. 7. Transfer function derived from hammer impact measurements for roller type 1 under a 440.000 N load per roller, illustrating the typical system response.

higher variability. This is because static stiffness is calculated from the slope of the load–displacement curve, making it highly sensitive to small errors in load increments. In contrast, the hammer impact method relies on resonance frequency, and its error is tied to the absolute load value, which is much less sensitive to such variations. Therefore, hammer impact measurement is preferred for this experimental setup.

2.6. Verification

To validate the accuracy of the test setup, rollers were replaced with steel bearing balls of diameters 3.000, 6.000, & 9.000 mm. For dry and smooth ball contacts, the Hertz contact model is well-established to be accurate [13]. Measurements using balls matched Hertzian theory within 5.000% across the load range [14], with stiffness standard deviations below 3.000%. These results confirm the test setup's accuracy and repeatability for the intended purpose.

Furthermore, the following actions were performed to investigate and minimize the uncertainty in the test setup:

- The mass of each component was measured using a calibrated scale.
- The load–displacement behavior of the springs was characterized using a calibrated load cell, with compression applied similarly to the actual test conditions.
- The influence of bolt tightening torque on the rail-to-mass connections was tested and found to be negligible, supporting the assumption of a rigid connection.
- Experimental modal analysis indicated a mean damping coefficient of 0.018 with a standard deviation of 0.008, justifying the assumption of an undamped test setup.

3. Results and discussion

This section begins with the results for the standard configuration: a 3.000 mm steel roller (roller type 1, Table 1) on a steel rail with Ra = 0.2 µm. This serves as the reference for subsequent analyses. Then, variations in the following parameters are investigated:

- Surface roughness of the rails: Ra = 0.2 µm and Ra = 0.03 µm
- Lubrication conditions: dry, oil-lubricated, and grease-lubricated contacts
- Roller geometry:diameter and length (D = 1.5, 3.0, 6.0, &9.0 mm, L = 1.4, 2.0, 2.2, 2.8, 4.0, 4.4, &8.8 mm)
- Roller material: bearing steel (1.3505), stainless steel (1.4034), and ceramic (Si_3N_4)

Finally, the experimental data is compared with theoretical predictions, and an empirical model is derived based on the measured results.

3.1. Stiffness of the reference roller configuration

The stiffness of a roller as a function of load is presented in Fig. 8.Across 10 repetitions, the total spread in measured stiffness is less than 5.000% at low loads and decreases to below 1.000% ($\sigma = 5.000 \cdot 10^4$ N/m) at higher loads.

3.2. Surface roughness

Fig. 8 illustrates the impact of surface roughness on stiffness. As roughness increases, stiffness decreases: the rail with Ra = 0.03 µm is considerably stiffer than the one with Ra = 0.2 µm. These test results show that surface roughness has a significant effect on the stiffness of

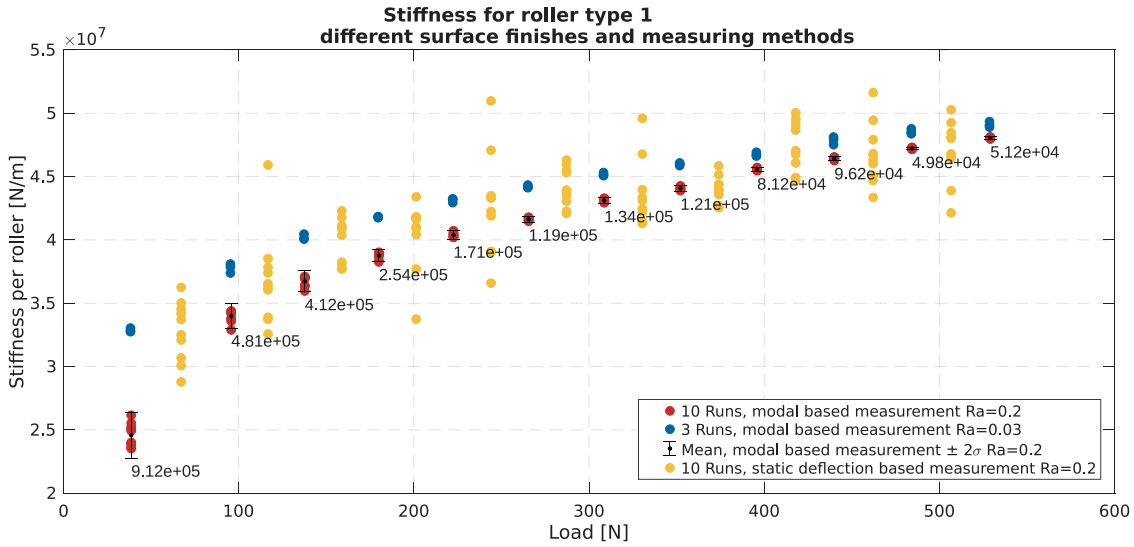

Fig. 8. Measured load-stiffness relation of a 3.000 mm steel roller on a steel rail with Ra = 0.2 µm.

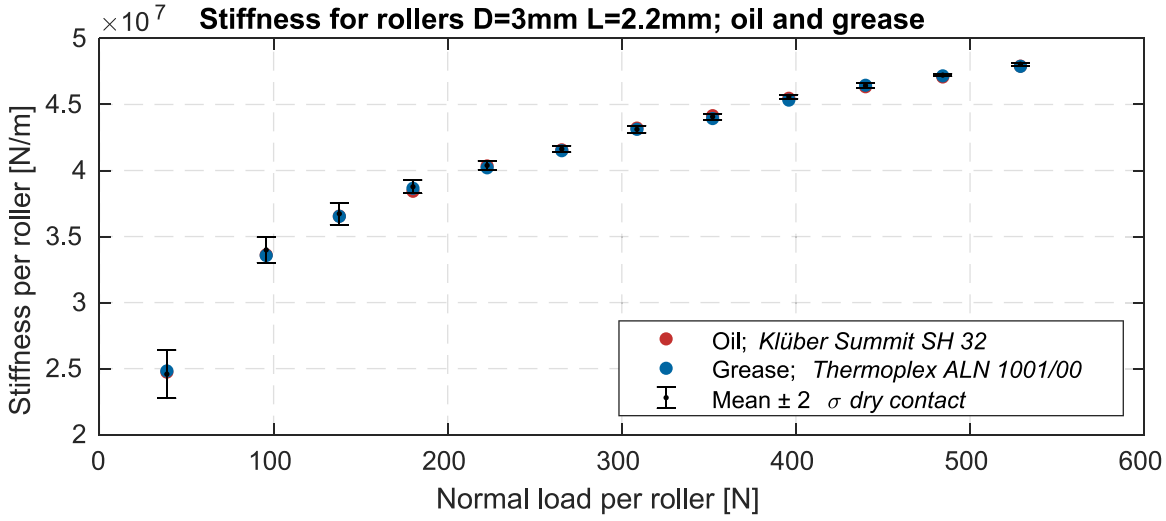

Fig. 9. Hammer impact data: Load-stiffness relation for roller type 1 under normal conditions; Mean values for rollers with different lubrication conditions.

a roller bearing in engineering practice. With increased roughness, the standard deviation of the measurements increases, particularly under low load conditions. This is attributed to the smaller contact area at lower loads, which increases the impact of individual roughness peaks. In Section 3.6, an empirical curve-fit model of the complete measurement dataset is presented, in which the influence of surface roughness on stiffness is explicitly included.

Flat rails are ground along their length during manufacturing, this process was also used to control the surface roughness. Tests were performed to evaluate whether the roller's orientation relative to the grinding direction affects the stiffness. As reported in [14], no significant effect of roller orientation was observed.

3.3. Lubrication conditions

Fig. 9 shows the stiffness per roller as a function of the normal load for rollers under various lubrication conditions. Tests with oil (*Klüber Summit SH 32* [15]) and grease (*Lubcon Thermoplex ALN 1001/00* [16]) applied to the roller-rail contact show no significant effect on stiffness or damping under stationary conditions (i.e. non-rolling) [14]. Since the rollers were not rolling, hydrodynamic pressure buildup, which could affect stiffness, was not observed.

3.4. Roller geometry

Roller length. Fig. 10(a) shows the load-stiffness relation per contact length (L_{we}) for rollers of varying lengths. A clear trend can be observed: the stiffness per contact length decreases as the roller length increases. This indicates that the roller edges contribute additional stiffness, an effect commonly referred to in the literature as *end effects* [17].

Roller diameter. There is no consensus on whether roller diameter significantly affects the load-stiffness relationship [1]. For some relationships, such as that of Tripp, the influence of the roller diameter cancels out when the rail and roller have identical elastic material properties. The relative influence of surface defects is expected to vary with roller diameter.

Fig. 10(b) presents the load-stiffness relation per contact length for rollers with diameters of 1.5, 6, & 9 mm. The data suggest a decrease in stiffness with increasing roller diameter. However, the roller length varied across experiments with different diameters due to the unavailability of suitable test specimens. Since roller length significantly influences stiffness, as shown in the previous section, no definitive conclusions can be drawn about the effect of diameter from this dataset.

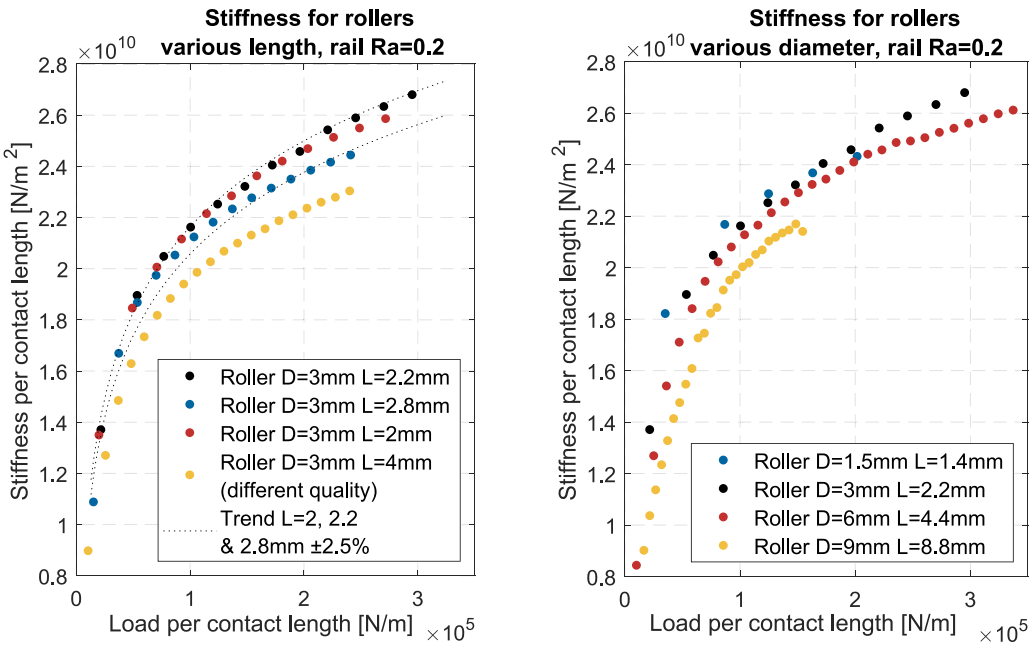

(a) rollers type 1, 5, 7, & 6; variation of length

(b) rollers type 2, 1, 3, & 4; variation of diameter

Fig. 10. Hammer impact data: Load-stiffness relation; Mean values for various geometries.

3.5. Roller material

Existing empiric load-stiffness relations are based on experiments with steel rollers. However, other materials, such as stainless steel (1.4034) and ceramic (Si_3N_4), are also used in some applications. These materials were tested and compared with steel rollers.

Ceramic rollers. Fig. 11(a) shows that ceramic rollers are stiffer than bearing steel rollers of the same length. This is expected, as deformation is influenced by the effective modulus of elasticity, which is higher for ceramics [13].

Fig. 11(b) shows that stainless steel rollers exhibit considerably higher stiffness than bearing steel rollers of the same length. This finding is unexpected, as the Young's modulus of stainless steel (200.000 GPa) is lower than that of bearing steel (210.000 GPa). The rollers have identical profiling and contact lengths, and the variance in the stainless steel measurements is consistent with other tests.

One possible explanation for this result is the lower hardness of stainless steel, which allows plastic deformation at higher loads. This deformation enables the roller to conform more effectively to the roughness profile of the rail, thereby increasing the effective contact area and, consequently, the measured stiffness. This hypothesis is supported by measurements on mirror finish rails (Ra = 0.03 µm), where the difference between stainless steel and bearing steel rollers is reduced, suggesting that surface roughness plays a role in this behavior.

In addition, the plastic deformation in stainless steel may induce local work hardening, increasing the material's effective stiffness beyond its nominal elastic properties. This mechanism could further contribute to the higher observed stiffness, particularly at elevated loads where yielding occurs locally in the contact zone.

Overall, this is an unexpected result, as material hardness and work hardening are not typically considered parameters of interest in conventional stiffness models [13], which assume purely elastic contact behavior.

3.6. Curve-fit model

This study tested eight roller types with variations in diameter, length, and Young's modulus. The rollers were placed between the rails with surface roughness values of Ra 0.2 µm and Ra 0.03 µm. From these measurements, a curve fit was developed to describe the stiffness of the roller as a function of length and external load.

Rail roughness Ra = 0.2 µm. Fig. 12 shows all measurements performed with steel rollers on rails with Ra = 0.2 µm. A least-squares logarithmic fit, described in Eq. (5), is shown, with most of the data points falling within a ±10% range of the fit.

3.7. Measurement results vs. analytical model

Fig. 12 compares the measured stiffness values for eight roller configurations with theoretical predictions based on the derivative of Tripp's load–deflection relationship [18]. Detailed calculations are provided in [14].

The curve-fit model accurately captures the measured dataset within a ±10% range. However, both the Tripp and Palmgren models show significant deviations from the experimental data.

As expected from the literature, the Tripp model serves as a *upper bound* for the measured stiffness values, as it assumes ideal conditions. At low loads, the measured stiffness is significantly lower than Tripp's predictions, primarily due to surface roughness, which reduces the effective contact area and amplifies local deviations.

Ra = 0.03 µm. Fig. 13 presents all measurements performed with steel rollers on rails with Ra = 0.03 µm. Similarly, most data points fall within a ±10% range of the fit described by Eq. (6).

$$k_{Ra_{0.2}} = 5.151 \cdot 10^9\ \mathrm{N/m^2}\ \ln\frac{P/L_{we}}{1.800 \cdot 10^3\ \mathrm{N/m}}\ L_{we} \tag{5}$$

$$k_{Ra_{0.03}} = 3.230 \cdot 10^9\ \mathrm{N/m^2}\ \ln\frac{P/L_{we}}{1.004 \cdot 10^2\ \mathrm{N/m}}\ L_{we} \tag{6}$$

4. Conclusions

- The proposed test setup and method yield accurate and repeatable results in order to investigate roller stiffness, as demonstrated by the low measurement spread.

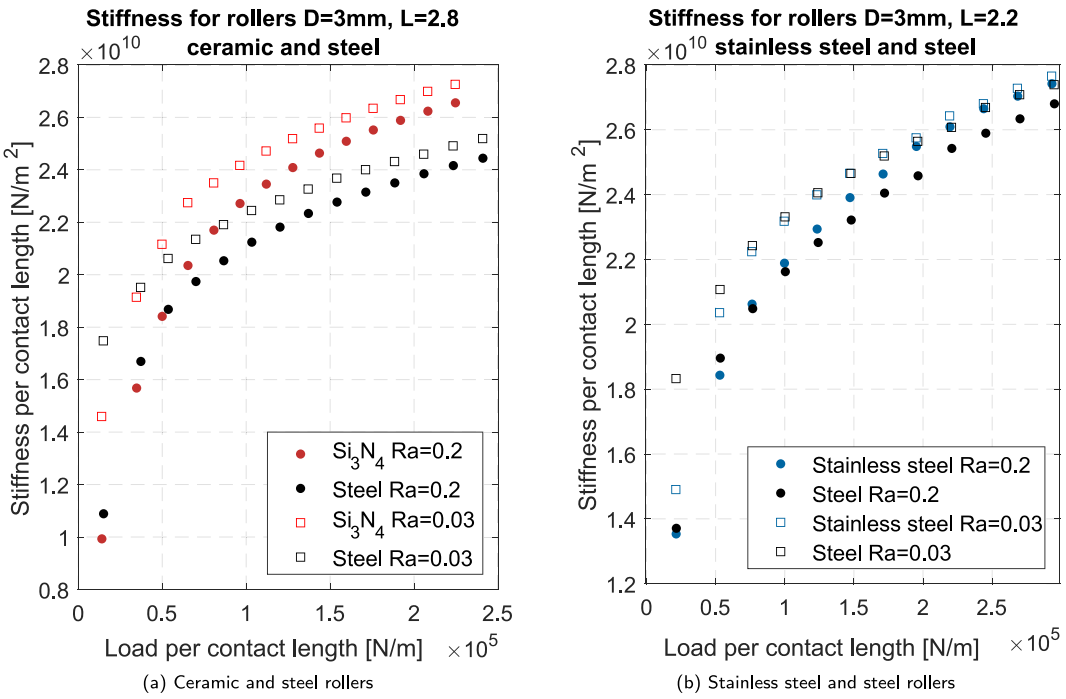

Fig. 11. Hammer impact data: Load-stiffness relation; Mean values for different surface finishes.

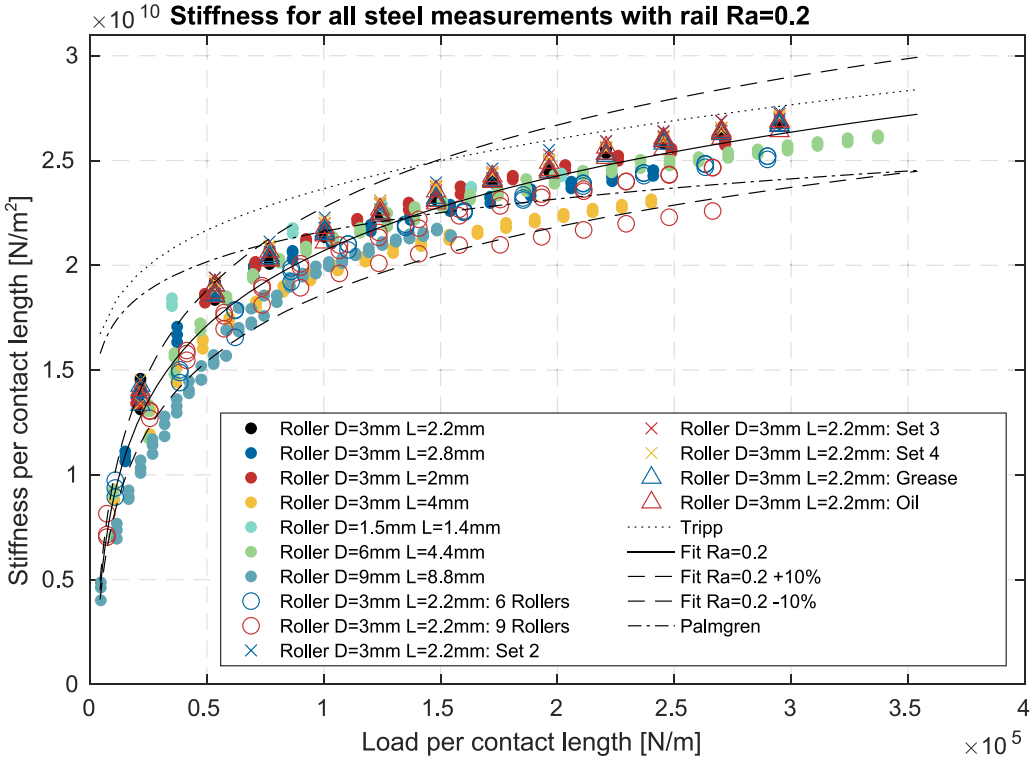

Fig. 12. Hammer impact data: Load-stiffness relation of all steel rollers with rails of Ra = 0.2 μm; Mean values for various geometries and conditions. Curve fit of Eq. (5).

- Surface roughness significantly affects roller contact stiffness, particularly at low loads, with the observed magnitude aligning with the predictions of Greenwood and Tripp [19].
- Eqs. (5) and (6) provide practical engineering estimates for roller stiffness between two rails with approximately 10.000% accuracy; the Tripp model serves as an idealized upper bound for comparison.
- Roller length has a significant effect on stiffness: longer rollers exhibit higher contact stiffness. However, stiffness does not scale linearly with length due to *end effects*, which result in higher stiffness per contact length for shorter rollers.
- No significant effect of roller diameter on contact stiffness was observed. However, the lack of test samples isolating diameter as a variable somewhat limits this conclusion.

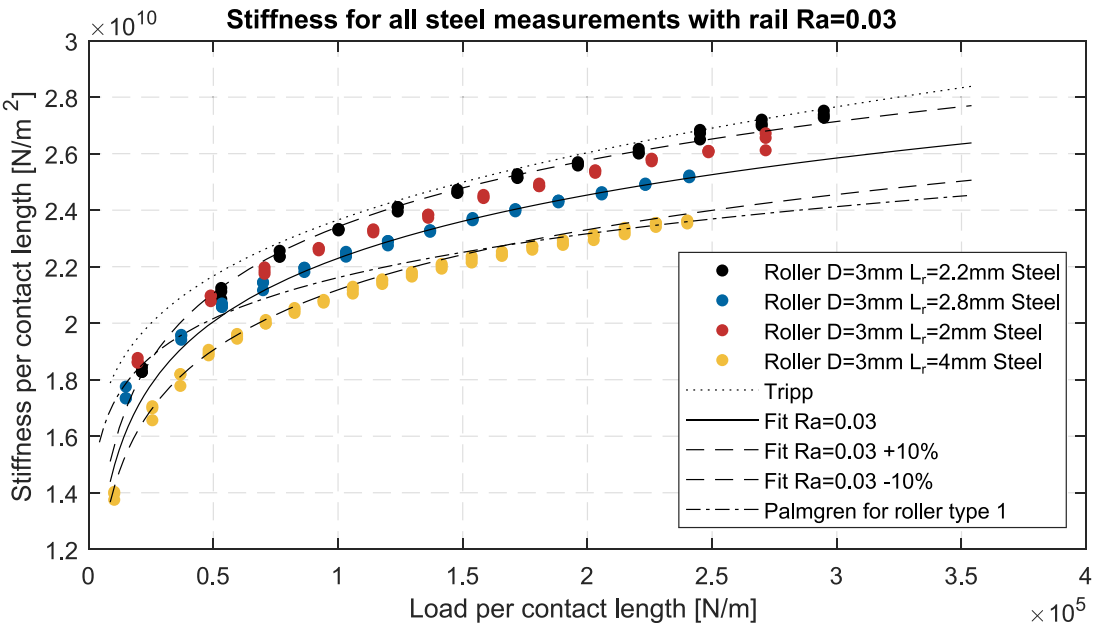

Fig. 13. Hammer impact data: Load-stiffness relation of all steel rollers with rails of Ra = 0.03 µm; Mean values for different geometries. Curve fit of Eq. (6).

Table 1
Parameters of the rolling elements used in the experiments. Surface roughness, cylindricity and circularity are based on measurements on three rollers.

Type	D mm	L_{we} mm	L_r mm	E GPa	ν (–)	Material number	Hardness min HRC	Roughness Ra µm	Cylindricity µm	Circularity µm
1[a]	3.00	1.793	2.20	210	0.29	Bearing steel (1.3505)	60	0.028	0.727	0.383
2	1.50	1.104	1.40	210	0.29	Bearing steel (1.3505)	60	–	–	–
3	6.00	3.805	4.40	210	0.29	Bearing steel (1.3505)	60	0.031	0.423	0.222
4	9.00	8.309	8.80	210	0.29	Bearing steel (1.3505)	60	0.034	0.463	0.227
5	3.00	2.569	2.80	210	0.29	Bearing steel (1.3505)	60	–	–	–
6	3.00	3.734	4.00	210	0.29	Bearing steel (1.3505)	60	0.080[b]	3.467	2.212
7	3.00	1.947	2.00	210	0.29	Bearing steel (1.3505)	60	–	–	–
8	3.00	2.756	2.80	300	0.26	Silicon nitride (Si_3N_4)	90	–	–	–
9	3.00	1.804	2.20	200	0.28	Stainless steel (1.4034)	54	–	–	–

[a] Based on measurements on 6 rollers.
[b] Based on measurement on a single roller.

Table 2
Setup components. All setup components are standard machine elements.

Component	Description	Type	Standard	Material
1	Blind flange (disc)	DN150-PN16	DIN 2527	Stainless steel (1.4307)
2	Guide way rail, see Fig. 14	PM O-92025 × 100	–	Bearing steel (1.3505)
3	Threaded rod	M10 - 8.8	DIN 976	Steel, galvanized
4	Washer	11X34 (M10) 100 HV	ISO 7094	Steel, galvanized
5	Star knob nut	BK38.0048.04010	–	Polyamide, brass insert
6	Hexagon head screw (torque 20.000 N m)	M8x40 - 12.9	ISO 4762	Steel, black oxide
7	Compression spring	FIBRO 241.14.32.038	ISO 10243	Steel 50CrV4

- Material hardness appears to influence stiffness in roller-rail contacts on Ra = 0.2 µm rails, with lower roller hardness improving contact conformation and increasing effective stiffness.
- Under static, non-rolling conditions, lubrication does not influence roller contact stiffness. However, rolling conditions were not investigated in this study and should be addressed in future work, particularly in relation to surface roughness and lubrication effects.

CRediT authorship contribution statement

David Onno Wijnberg: Writing – review & editing, Writing – original draft, Conceptualization. **Rob Eling:** Writing – review & editing, Investigation, Conceptualization. **Ron A.J. van Ostayen:** Writing – review & editing, Supervision, Conceptualization.

Declaration of competing interest

The authors declare the following financial interests/personal relationships which may be considered as potential competing interests: D.O. Wijnberg as a Intern received equipment and materials. Rob Eling was employed at the company and was D.O. Wijnberg his supervisor reports financial support and equipment, drugs, or supplies were provided by PM B.V. If there are other authors, they declare that they have no known competing financial interests or personal relationships that could have appeared to influence the work reported in this paper.

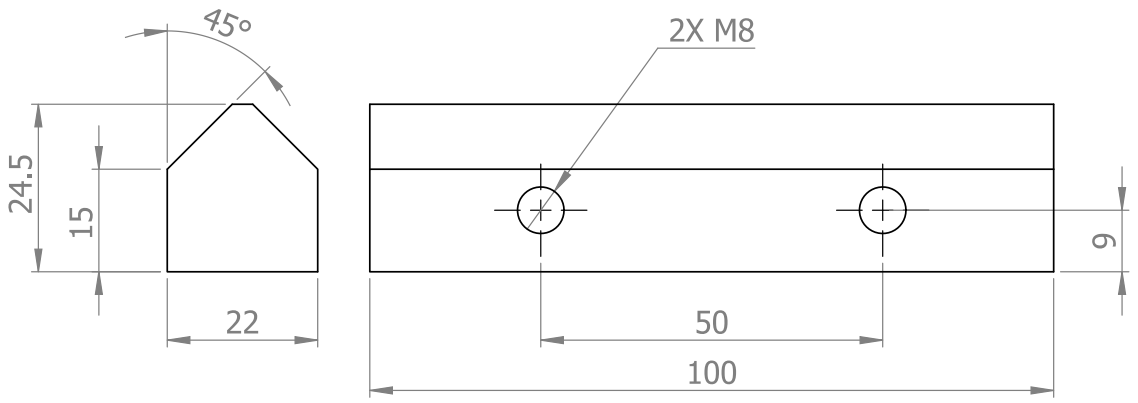

Fig. 14. Dimensions of the rails used in the experiments. PM B.V. *O-92025 × 100*. The rails are made out of bearing steel (1.3505).

Data availability

Data will be made available on request.

References

[1] Teutsch R, Sauer B. An alternative slicing technique to consider pressure concentrations in non-hertzian line contacts. J Tribol 2004;126(3):436–42. http://dx.doi.org/10.1115/1.1739244.

[2] Palmgren A. Ball and roller bearing engineering. Philadelphia: SKF industries; 1959, URL: http://www.worldcat.org/oclc/19827891.

[3] Sherif A. Determination of ball and roller compliances using a vibration measuring technique. J Tribol 1995;117(3):553–7. http://dx.doi.org/10.1115/1.2831290.

[4] Nakhatakyan FG. Mechanics of contact approach of elastic bodies in hertz problem. J Mach Manuf Reliab 2010;39(5):444–51. http://dx.doi.org/10.3103/S1052618810050079.

[5] Harris TA, Anderson WJ. Rolling bearing analysis. 5th editio. J Lubr Technol 2006;89(4):521. http://dx.doi.org/10.1115/1.3617048.

[6] Hong SW, Tong VC. Rolling-element bearing modeling: A review. Int J Precis Eng Manuf 2016;17(12):1729–49. http://dx.doi.org/10.1007/s12541-016-0200-z.

[7] Nikpur K, Gohar R. Deflexion of a roller compressed between platens. Tribol Int 1975;8(1):2–8. http://dx.doi.org/10.1016/0301-679X(75)90037-7.

[8] Lundberg G. Elastische berührung zweier halbräume. Forsch Geb Ingenieurwesens 1939;10(5):201–11. http://dx.doi.org/10.1007/BF02584950.

[9] Hoeprich MR, Zantopulos H. Line contact deformation: A cylinder between two flat plates. J Tribol 1981;103(1):21–5. http://dx.doi.org/10.1115/1.3251609.

[10] McCallion H, Truong N. The deformation of rough cylinders compressed between smooth flat surfaces of hard blocks. Wear 1982;79(3):347–61. http://dx.doi.org/10.1016/0043-1648(82)90324-6.

[11] Hu Y, He L, Luo Y, Tan AC, Yi C. Contact load calculation models for finite line contact rollers in bearing dynamic simulation under dry and lubricated conditions. Lubricants 2025;13(4). http://dx.doi.org/10.3390/lubricants13040183.

[12] The MathWorks I. MATLAB. 2021, URL: https://www.mathworks.com.

[13] Johnson KL. Contact Mechanics. Cambridge University Press; 1985, http://dx.doi.org/10.1201/b17110-2, URL: https://doi.org/10.1017/CBO9781139171731.

[14] Wijnberg DO. On the Stiffness of Linear Roller Bearings (Master thesis), Delft University of Technology; 2021, URL: https://resolver.tudelft.nl/uuid:ee19fa63-6fac-42c4-8143-8a5fbfa0f3fa, doi: https://resolver.tudelft.nl/uuid:ee19fa63-6fac-42c4-8143-8a5fbfa0f3fa.

[15] Technical information klüber summit SH 32, 46, 68, 100. 2014, -, URL: https://domxoloda.ru/oils/docs/Summit-SH.pdf.

[16] Technical information THERMOPLEX ALN 1001 eng. 2008, -, URL: https://www.ontrium.com/get.aspx?id=696826.

[17] Tudose L, Tudose C. Roller profiling to increase rolling bearing performances. IOP Conf Ser Mater Sci Eng 2018;393(1):012002. http://dx.doi.org/10.1088/1757-899X/393/1/012002.

[18] Tripp J. Hertzian Contact in Two and Three Dimensions. Technical Report, NASA; 1985, p. 24, URL: https://ntrs.nasa.gov/citations/19850024018.

[19] Greenwood JA, Tripp JH. The elastic contact of rough spheres. J Appl Mech Trans ASME 1964;34(1):153–9. http://dx.doi.org/10.1115/1.3607616.